Energy & Environmental Science

RSC Publishing

PAPER

View Article Online
View Journal | View Issue

Cite this: *Energy Environ. Sci.*, 2013, **6**, 3088

Low-temperature, solution-processed, layered V_2O_5 hydrate as the hole-transport layer for stable organic solar cells†

Gerardo Terán-Escobar, Jonas Pampel, José M. Caicedo and Mónica Lira-Cantú*

Received 1st July 2013
Accepted 29th July 2013

DOI: 10.1039/c3ee42204f

www.rsc.org/ees

Layered V_2O_5 hydrate has been applied as the hole transport layer (HTL) in organic solar cells (OSCs). V_2O_5 is obtained from a sodium metavanadate solution in water under ambient conditions, resulting in a final thin film of formula $V_2O_5 \cdot 0.5H_2O$. The 0.5 water molecules are not removed from the V_2O_5 layered structure unless the sample is heated above 250 °C, which makes the thin film highly stable under real working conditions. The HTL was used in OSCs in the normal and the inverted configurations, applying metallic Ag as the back-metal electrode in both cases. Fabrication of both OSC configurations completely by solution-processing printing methods in air is possible, since the Al electrode needed for the normal-configuration OSC is not required. The work function (WF) and band gap energy (BG) of the V_2O_5 thin films were assessed by XPS, UPS and optical analyses. Different WF values were observed for V_2O_5 prepared from a fresh V_2O_5–isopropanol (IPA) solution (5.15 eV) and that prepared from a 24 h-old solution (5.5 eV). This difference is due to the gradual reduction of vanadium (from V^{5+} to V^{4+}) in IPA. The OSCs made with the V_2O_5 thin film obtained from the 24 h-old V_2O_5–IPA solution required photo-activation, whereas those made with the freshly obtained V_2O_5 did not. Outdoor stability analyses of sealed OSCs containing a V_2O_5 HTL in either configuration revealed high stability for both devices: the photovoltaic response at T_{80} was retained for more than 1000 h.

Broader context

Organic Solar Cells (OSCs) have achieved an impressive increase in power conversion efficiency in the past few years, with values above the 12% range. Yet, in order to be competitive with existing energy sources from fossil fuels and modern inorganic photovoltaic technologies, OSCs must reduce fabrication costs and improve its energy payback time (EPBT). To achieve the latter, the fabrication of OSCs by large scale, solution processing methods applying inexpensive, low temperature techniques is required. An important aim is the exclusion of toxic organic solvents, being water-based or alcohol-based solutions is highly desired. In this work, a layered V_2O_5 hydrate has been applied as the hole transport layer in stable OSCs. V_2O_5 is obtained from the dissolution of sodium metavanadate in water under ambient atmospheric conditions, resulting in a final thin film with the $V_2O_5 \cdot 0.5H_2O$ formula. OSCs with normal and inverted configuration applying metallic Ag as the back metal electrode in both cases have been fabricated. The use of a Ag electrode eliminates the need for a highly reactive work function metal electrodes (Al, Ca) for the normal configuration OSC, and permits the fabrication of both OSC configurations completely by solution processing printing methods in air. Outdoor stability analyses of sealed devices showed high stability, maintaining the photovoltaic response at T_{80} for more than 1000 h.

1 Introduction

The predicted maximum power conversion efficiency (PCE) of organic solar cells (OSCs) has been empirically estimated to be 10 to 12%, but theoretical calculations suggest that values of 20 to 24% could be achieved, which are comparable to those of crystalline Si solar cells.[1] However, OSCs must also be cost-competitive and show long lifetimes. The former requires inexpensive methods for large-scale fabrication, including solution-processing techniques such as roll-to-roll compatible printing techniques.[2–8] Ideally, a single printing method would be used to continuously and rapidly process all layers; unfortunately, no such process exists yet and therefore, multiple techniques must be employed. Additionally, the envisaged mass-production of OSCs indicates that toxic organic solvents will have to be replaced with non-toxic, alcohol or water-based solutions and inks. Interestingly, a few cases of partial or complete roll-to-roll fabrication methods of OSCs with water-based inks have very recently been reported.[5,9–11]

Transition metal oxides (TMOs) have been employed in organic solar cells, especially TiO_2 and ZnO. Their most attractive feature is the possibility to be deposited by low temperature solution processing methods. Among them are

Catalan Institute of Nanoscience and Nanotechnology (ICN2), Campus UAB, Building ICN2, Bellaterra, Barcelona, E-0193, Spain, Consejo Superior de Investigaciones Cientificas (CSIC), Campus UAB, Building ICN2, Bellaterra, Barcelona, E-0193, Spain. E-mail: monica.lira@cin2.es; Fax: +34 937373606; Tel: +34 937374615

† Electronic supplementary information (ESI) available. See DOI: 10.1039/c3ee42204f

also V_2O_5,[12–21] NiO,[22–30] MoO_3,[31–35] WO_3[36–39] or Sb_2O_3.[40] These TMOs exhibit a wide range of energy level alignments,[41–44] good transparency as thin films, are easy to manipulate, and confer low-resistance ohmic contacts to the OSC.[45] Moreover, TMOs can enhance the adhesion to the active layer[8,16] and show higher stability to ambient atmosphere relative to PEDOT:PSS, which has been shown to be detrimental for OSCs due to its high hygroscopicity and its acidic pH.[46–50] Additionally, the high power conversion efficiency requirement for future OSCs rely on small-molecule OSCs (SmOSCs)[39,40,51,52] and multi-junction or tandem solar cell (TmOSC) structures, whose PCE values presently range from 10–12%.[5,10,53–56] One interesting TMO is V_2O_5, which has been reported to be a good candidate for the HTL in OSCs. To date, V_2O_5 HTLs have been synthesised chiefly by multistep techniques. Examples include the suspension of V_2O_5 nanoparticulates obtained from the hydrolysis of vanadium(III) acetyl acetate[19] or the fabrication of a bronze V_2O_5 HTL from a suspension of the metal oxide obtained after the reaction between the metal powder and H_2O_2.[21] Among the most widespread fabrication methods is the application of sol–gels made from vanadium(V) oxytriisopropoxide (ViPr),[5,14,15,57,58] which is a compound known for its high toxicity, reactivity and cost.

Herein we present the synthesis, optimisation and application of water-based, solution processable V_2O_5 as the HTL in OSCs. The HTL was fabricated at low temperature in air without the need for any high temperature post-deposition treatments or multistep reactions. The water-based layered V_2O_5 hydrate is highly compatible with the fabrication of OSCs by large-area, low-cost, fast processing and high-throughput printing,[5,15] and also enables the preparation of ZnO/V_2O_5 recombination layers required for TmOSCs.[59] We demonstrate here that the application of the low-temperature water-based V_2O_5 solution can be tuned in order to fabricate OSCs in either the inverted or the normal configurations, on either glass or flexible substrates. Moreover, we have fabricated OSCs with both configurations applying only Ag as the back metal electrode. Thus, our OSCs can be made completely by solution-processing methods, as they do not require an Al electrode for the normal-configuration OSCs[10] and the Ag metal electrode can be deposited by established solution-processing printing techniques.[11] A careful optimisation of the V_2O_5 hydrate solution permitted to obviate the requirement for photo-activation of the solar cell in air.[19] Finally, the OSC devices also show good outdoor stability maintaining T_{80} for more than 1000 h.

2 Experimental section

2.1 Synthesis of TMOs

The TiO_2 solution was fabricated and deposited as previously reported,[60] and the ZnO nanoparticles were synthesised following the Pacholski method[61] and deposited by spin coating at 1000 rpm. The V_2O_5 hydrate solution was obtained using an adapted version of Livage's method.[62] Briefly, 4.5 g of sodium metavanadate ($NaVO_3$) are dissolved in 100 mL of deionised water by heating the mixture at 90 °C with stirring. The resulting transparent solution is passed through a cation-exchange resin (DOWEX 2x-100, Aldrich) to obtain metavanadic acid (HVO_3) as a yellow solution, which is stored in a closed glass flask under an ambient atmosphere. As the solution ages, it becomes yellowish-orange, indicating the presence of condensed species such as decavanadates ($[V_{10}O_{28}]^{6-}$). Finally, the orange solution changes to dark red, which is characteristic of the V_2O_5 hydrate (gel). The condensation and aging of the solution occurs over ~20 days, after which, the viscous hydrate solution stabilises and is ready to use. A bright red vanadium pentoxide $V_2O_5 \cdot nH_2O$ gel is obtained. For the inverted OSC a 1 : 1 mixture of V_2O_5 hydrate (9 mg mL^{-1}) in isopropanol (IPA) was spin-coated at 1000 rpm, and then annealed at 120 °C for 5 min. For the normal configuration OSCs the V_2O_5 solution was spin coated at 1000 rpm directly from the solution without the aid of the IPA.

2.2 Solar cell fabrication

The response of the solar cells was independent of the used substrate (ITO or FTO). All the flexible substrates were made on a PET/ITO transparent film. Substrates of FTO on glass were supplied by SOLEMS (resistance: 70 to 100 ohms). PET/ITO substrates were brought from Aldrich (resistance: 35 ohms). The substrates were cleaned with a water–soap solution, rinsed with deionised water, ultrasonicated in ethanol (99%), dried under N_2 flux and finally, ozone treated in a UV-surface decontamination system (Novascan, PSD-UV) connected to an O_2 supply. The OSCs were fabricated in either the *normal configuration* (FTO/V_2O_5/P3HT:PCBM/TiO_2/Ag) or the *inverted configuration* (FTO/TiO_2/P3HT:PCBM/V_2O_5/Ag). TiO_2 was used on glass/FTO substrates and was replaced by ZnO in order to fabricate flexible OSCs on ITO/PET (Aldrich). The bulk heterojunction blend comprised a 1 : 0.8 mixture of regioregular P3HT (Merck, 98%) and PCBM (Solenne, 99.5%) that was dissolved in dichlorobenzene (Sigma-Aldrich). The blend was spin coated at 1000 rpm, affording a 200 to 250 nm-thick P3HT:PCBM film. The devices were subsequently annealed at 120 °C for 5 min in air. A 100 nm-thick Ag back metal electrode was deposited by thermal evaporation in an evaporation system (Auto 306, Broc Edwards) with a base pressure of 10^{-7} torr at a deposition rate of 1 Å s^{-1}. The final active area was 0.2 cm^2. The solar cells were sealed by applying a two-component adhesive (ThreeBond, 30Y-727 and 31x-167-2), which was mixed in a 1 : 1 ratio and cured under UV light for 10 min.

2.3 Characterisation

The thicknesses of the polymer layers were measured using a Nanopics-2100 from Nanopics profilometer and by SEM (Quanta FEI 200 FEG-ESEM). Optical measurements were performed using a UV-vis spectrophotometer (UV 1800, Shimadzu). Grazing incidence X-ray analyses were done using a Rigaku unit and measured between 5° and 80°. TGA analyses were done using an STA 449 F1 Jupier (Netzsch). Contact angles were analysed using a DSA 100 (KRUSS). XPS was done with the Al κα (1486.6 eV). All spectra were adjusted according to the value of the C 1s peak at 284.4 ± 0.1 eV. The UPS were obtained using a He lamp (He I 21.2 eV) at an experimental resolution of 0.15 eV. The samples were biased at −5 V.

2.4 Photovoltaic characterisation

The solar simulation was performed on a KHS1200 (Steuernagel Solarkonstant) equipped with an AM1.5 filter for all characterisations (100 mW cm^{-2}, AM1.5G, 72 °C). The equipment was calibrated according to the ASTM G173. *IV*-curves were measured using a Keithley 2601 multimeter. Light intensity was 100 mW calibrated with a Zipp & Konen CM-4 pyranometer, which was used constantly during measurements to set light intensity, and a calibrated S1227-1010BQ photodiode from Hamamatsu was also applied for calibration before each measurement. IPCE analyses were done with a QE/IPCE measurement System from Oriel (from 300 to 700 nm; at 10 nm intervals). The results were not corrected for any intensity losses due to light absorption or reflection by the glass support.

2.5 Outdoor stability analyses

The outdoor stability analyses were done following the ISOS-1 procedures[63] at the Laboratory of Nanostructured Materials for Photovoltaic Energy of the Catalan Institute of Nanoscience and Nanotechnology (ICN2-CSIC), located in Barcelona, Spain (41.30° N 2.09° W), using a solar tracking positioning system. The system comprises a large dual axis-controlled platform with fully automated motors, which enables turning of the tracker hour angle up to 100° (which translates to nearly 7 hours of perpendicular solar tracking) and turning of the tracker elevation angle from 15° to 90° (which enables full tracking of solar elevation). We developed in-house software to control the photovoltaic response of sixteen solar cells at the same time and to continuously monitor light irradiation, temperature and relative humidity over time. *IV*-curves were measured using a 2602A dual-channel SMU multimeter and a 3700 series switch/multimeter (both from Keithley). PCE values were calculated using the maximum daily irradiance level. The light irradiation was measured with a Zipp&Konen CM-4 pyranometer. The temperature and relative humidity were monitored with a combined sensor (Theodor Friedrichs).

3 Results and discussion

3.1 Optimisation of the V_2O_5 layer: concentration and layer thickness

V_2O_5 hydrate is obtained from an aqueous solution of sodium metavanadate ($NaVO_3$). During synthesis, the $NaVO_3$ dissolved in water is converted into metavanadic acid (HVO_3) *via* cation-exchange. A condensation process over time results in the formation of decavanadates ($[V_{10}O_{28}]^{6-}$), and finally, a dark red solution is obtained, corresponding to vanadium pentoxide hydrate ($V_2O_5 \cdot nH_2O$, where n varies). The variable water molecules in V_2O_5 hydrate are partially eliminated when the $V_2O_5 \cdot nH_2O$ thin film is formed on the glass/FTO substrate. The number of water molecules (n) in the formula $V_2O_5 \cdot nH_2O$ ranges from 0 to 2.2, depending on the annealing temperature: below 120 °C, $n = 1.6$; from 120 to 250 °C, $n = 0.5$; from 250 to 320 °C, $n = 0.1$; and annealing above 320 °C promotes the total elimination of water ($n = 0$) and the crystallisation of V_2O_5 into its rhombic crystalline phase.[64,65]

The V_2O_5 film used in this work was prepared by spin coating and the substrate was then treated at 120 °C for several minutes before being applied to the OSCs. The final formula of the thin

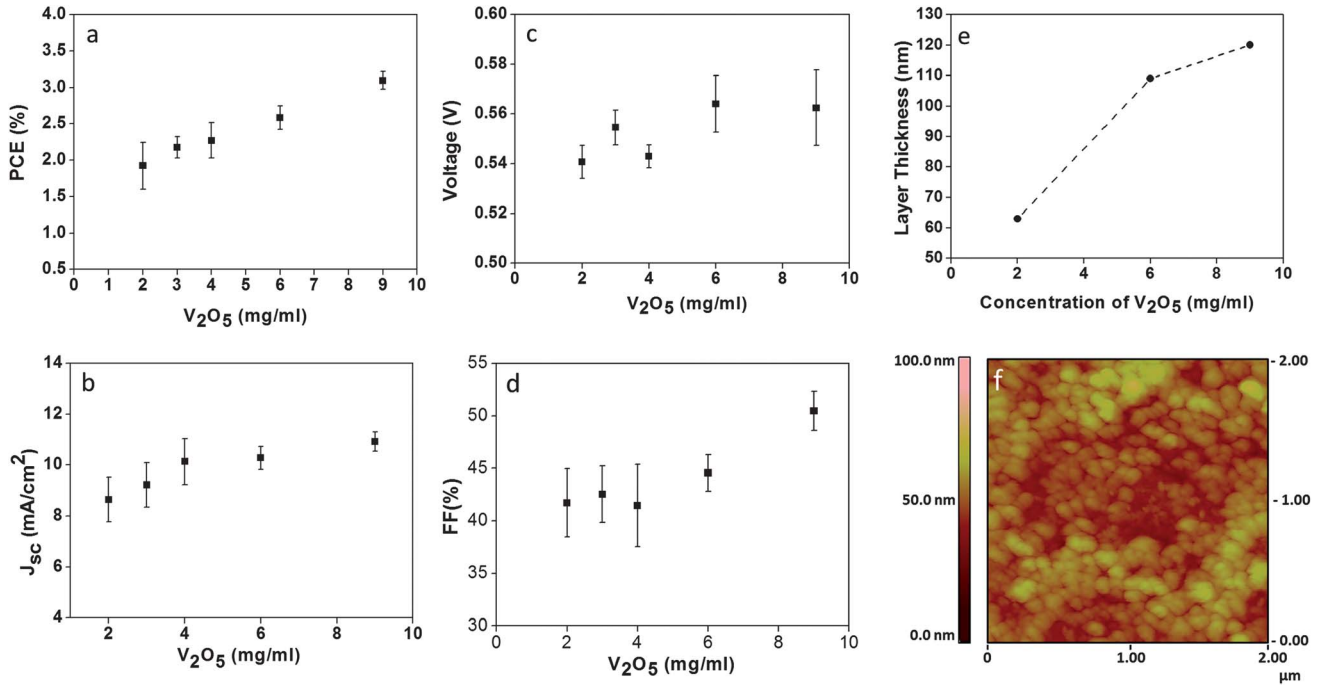

Fig. 1 Optimisation of the concentration of the V_2O_5 hydrate solution used to create the hole transport layer in an inverted organic solar cell (glass/FTO/TiO_2/P3HT:PCBM/V_2O_5/Ag). (a) PCE (%) and (b) J_{sc} (mA cm^{-2}). Measurements made at 100 W cm^{-2} AM1.5G. (c) V_{oc} and (d) FF (%), (e) layer thickness *vs.* V_2O_5 concentration and (f) AFM analyses of the V_2O_5 thin film made with a concentration of 9 mg mL^{-1}.

film is $V_2O_5 \cdot 0.5H_2O$ (the number of water molecules was calculated from the TGA analyses performed in air). Once the films have been prepared, the water molecules can only be removed if the film is heated above 250 °C. However, under real working conditions the OSCs will never reach those temperatures and therefore, the water in the V_2O_5 interlayer can be considered stable.

Fig. 1 shows the photovoltaic response of inverted organic solar cells with the glass/FTO/TiO_2/PCM:P3HT/V_2O_5/Ag configuration, depending on the V_2O_5 concentration. For the fabrication of inverted devices, the deposition of V_2O_5 on top of the active P3HT:PCBM layer requires mixing of V_2O_5 hydrate with isopropanol (IPA) to improve adherence. The optimum ratio of V_2O_5 to IPA was found to be 1 : 1 (as determined by contact angle measurements; see ESI Fig. S1†). The solution obtained was then spin-coated at 1000 rpm in an ambient atmosphere, and finally, heated at 120 °C for 5 min. There is a clear improvement on the photovoltaic response of the device (*ca.* in FF, J_{sc} and PCE) when the concentration of the oxide is increased from 2 mg mL^{-1} to 9 mg mL^{-1}, as observed in Fig. 1. The PCE and FF increase and ultimately stabilise at 3% and 50%, respectively. As the FF increased, the J_{sc} also stabilised at a V_2O_5 concentration of 9 mg mL^{-1}. Increasing the photovoltaic response by increasing the concentration of V_2O_5 above these values was not achievable due its limited solubility. Thus, the optimal value chosen for fabrication of the inverted OSCs was 9 mg mL^{-1}. An increase in the thin film layer thickness was also observed when raising the concentration of the oxide from 2 mg mL^{-1} to 9 mg mL^{-1}, with values ranging from 60 nm to 125 nm (as measured by SEM and profilometry, Fig. 1e). The possibility to fabricate thick film layers without compromising the photovoltaic performance of the device (*i.e.* by increasing series resistance) has also been observed by Brabec *et al.*[19] In our case, we attributed this response to the mixed ionic-electronic conductivity that characterises the $V_2O_5 \cdot 0.5H_2O$ thin film. Finally, Fig. 1f shows the atomic force microscopy (AFM) image, at a 2 mm × 2 mm scan size, of the thin film V_2O_5 made with a solution concentration of 9 mg mL^{-1}. A nanostructured surface with high surface roughness is observed for the thin film.

To compare the performance of our V_2O_5 HTLs with that of the most widely used HTL, PEDOT:PSS, we fabricated and assessed OSCs of both configurations. The devices were prepared on glass/FTO substrates (the fabrication of flexible OSCs applying the V_2O_5 HTL is also possible, see ESI Fig. S2†). Fig. 2 shows the *IV* curves and the IPCE spectra obtained for the devices. In all cases the ETL was ZnO. Table 1 shows the photovoltaic parameters obtained for the different OSCs; for comparison purposes, we have also included solar cells containing a TiO_2 ETL. The reported values are mean values from six samples. The best photovoltaic performance (PCE: 3%) was generally observed for the OSC fabricated on glass/FTO substrates, with TiO_2 as the ETL and V_2O_5 hydrate as the HTL. In this case, the OSCs employing the V_2O_5 hydrate resulted in better performance when compared to PEDOT:PSS. The OSCs with ZnO and V_2O_5 showed a very similar response with photovoltaic PCEs of *ca.* 2.5 to 2.6%. Our results indicate that a similar response can be achieved for OSCs with layered V_2O_5 hydrate when compared to the PEDOT:PPS HTL.

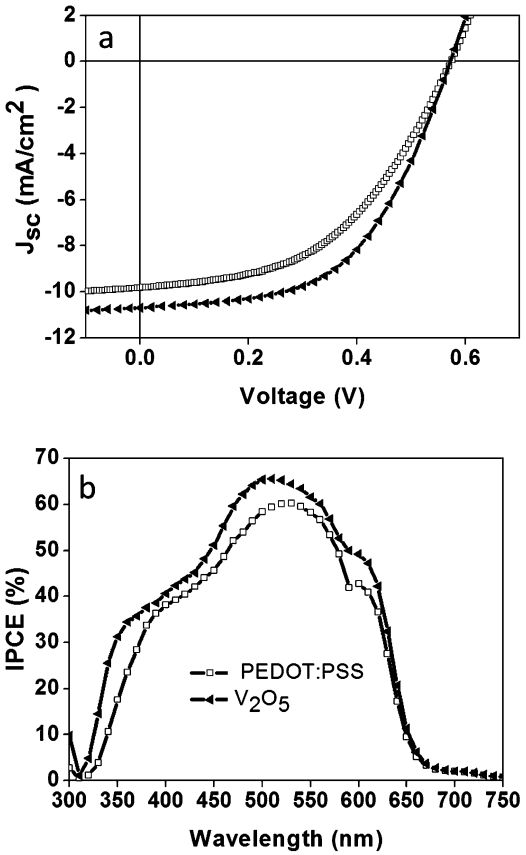

Fig. 2 *IV* curves (a) and the corresponding IPCE spectra (b) for the inverted configuration organic solar cell in glass/FTO/ZnO/P3HT:PCBM/V_2O_5/Ag and, for comparison purposes, similar cells containing PEDOT:PSS instead of V_2O_5. Measurements were taken at 100 mW cm^{-2} AM1.5G.

3.2 S-shape curve and photo-annealing of the inverted OSC in air

Fig. 3 shows the *IV*-curves and IPCE spectra obtained for our OSCs fabricated with fresh (1) and 24 hour-old (2) V_2O_5–IPA solutions. As observed, the OSC made with the fresh solution exhibited maximum photovoltaic performance directly after fabrication (Fig. 3a-(1)). In contrast, the OSC made with the 24 h-old solution (Fig. 3a-(2)) gradually improved with *IV*-cycles, ultimately reaching maximum performance (Fig. 3a-(3)). The corresponding IPCE analyses (see Fig. 3b) are in close agreement with the PCE values obtained for the OSCs. Besides the difference in IPCE intensity values, the most significant variations between the IPCE applying freshly prepared (1) and 24 h-old (2) V_2O_5–IPA solutions are observed in the wavelength region below 450 nm, corresponding to the adsorption of the semiconductor oxides (TiO_2, ZnO, V_2O_5, *etc.*).

Since the only difference in the fabrication of the two OSCs was the V_2O_5 HTL, we attributed the need for photo-annealing to the V_2O_5 thin film properties that are probably affected by the interaction between V_2O_5 with IPA.[62,66,67] Layered vanadium(v) oxides in their hydrated state tend to accommodate foreign molecules in their interlayer region,[64,66–68] including organic compounds such as alcohols.[69] Alcohols intercalate, *via* their –OH group, at the polar site of V_2O_5. In this partially reversible

Table 1 Photovoltaic parameters of inverted OSCs fabricated with hole transport layers of either V_2O_5 or PEDOT:PSS. The values are the mean from six samples. Measurements were taken at 100 mW cm^{-2} AM1.5G

Inverted configuration	V_{oc} (V)	J_{sc} (mA cm^{-2})	FF (%)	PCE (%)
Glass/FTO/TiO_2/P3HT:PCBM/PEDOT:PSS/Ag	0.557 ± 0.015	9.84 ± 0.43	45.43 ± 2.74	2.53 ± 0.17
Glass/FTO/TiO_2/P3HT:PCBM/V_2O_5/Ag	0.563 ± 0.015	10.69 ± 0.38	50.49 ± 1.90	3.09 ± 0.18
Glass/FTO/ZnO/P3HT:PCBM/PEDOT:PSS/Ag	0.543 ± 0.013	10.07 ± 0.37	45.06 ± 1.16	2.64 ± 0.12
Glass/FTO/ZnO/P3HT:PCBM/V_2O_5/Ag	0.540 ± 0.016	9.54 ± 1.10	47.20 ± 1.90	2.58 ± 0.22

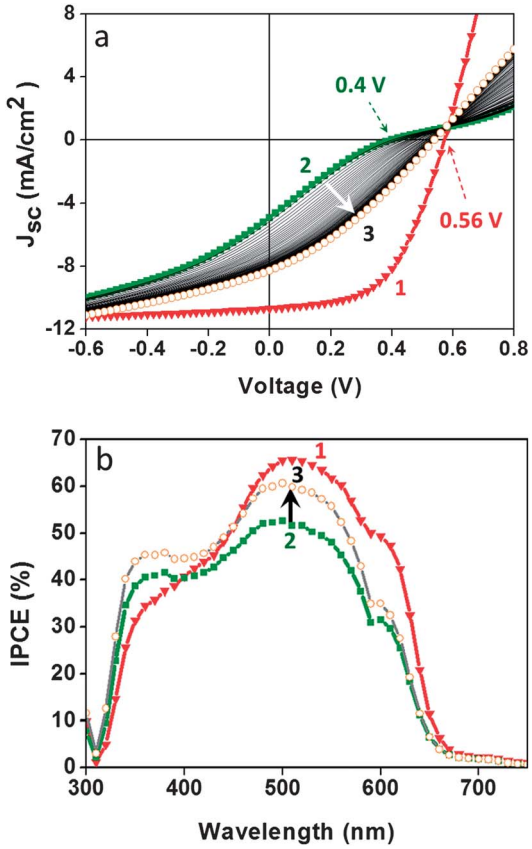

Fig. 3 Organic solar cells withV_2O_5 hydrate as the hole transport layer in the inverted configuration (glass/FTO/TiO_2/P3HT:PCBM/V_2O_5/Ag). Photovoltaic response of the cells fabricated from a freshly prepared (1) or a 24 h-old (2) V_2O_5–IPA solution. Using the fresh solution obviates the need for photo-activation of the device in air, as shown in the *IV*-curves and IPCE spectra from (2) to (3). Measurements were taken at 100 mW cm^{-2} AM1.5G.

reaction the H_2O molecules of V_2O_5 hydrate are exchanged with alcohol molecules, leading to the reduction of V_2O_5 from V^{+5} to V^{+4}. V_2O_5 reduces relatively quickly when in solution with organic molecules, as indicated by a gradual change in the colour of the solution from red (indicative of V^{5+}) to green (indicative of the reduction of V^{5+} to V^{4+}). Thus, the thin film obtained from the 24 h-old V_2O_5–IPA solution could be partially reduced and therefore photo-annealing is required in order to eliminate the undesirable shunts and inflection points (S-shape *IV* curve) and to achieve maximum power conversion efficiency.[4,70,71,80]

To understand the changes that we observed in the OSCs as a function of the freshness of the V_2O_5–IPA solution, we

Table 2 Binding energy values (in eV) of the main peaks in the XPS spectra of $V_2O_5 \cdot 0.5H_2O$ thin films obtained from fresh or 24 h-old solutions of V_2O_5–IPA[21,72–74]

Peak	Fresh (red)	24 h-old (green)	Assignment
$V2p_{3/2}$	516.20	516.20	V^{4+}
$V2p_{3/2}$	517.20	517.20	V^{5+}
$V2p_{1/2}$	524.75	524.70	V^{5+}
O 1s	529.95	529.90	O_2^-
O 1s	533.20	—	H_2O

characterised the V_2O_5 thin films by XPS, UPS and optical analyses.[76–78] Fig. 4a shows the XPS spectra of the $V_2O_5 \cdot 0.5H_2O$ thin films fabricated from the fresh (red) and 24 h-old (green) solutions. The binding energy (BE) values of the main peaks and their assignment are detailed in Table 2.

XPS analyses revealed only slight differences in the intensity of the spectra between the two films (see ESI Fig. S3†). Despite these small differences, the two thin films gave very similar XPS results: the main peaks of $V2p_{3/2}$ and $V2p_{1/2}$ were almost identical. The characteristic peaks of V_2O_5 are observed at 517 eV and 524 eV (corresponding to V^{5+}), and at 529.9 eV (the O 1s from the O^{2-} ions). The XPS plot was subject to a Lorentzian–Gaussian fitting: the region of the V^{5+} peak at 517 eV reveals a shoulder at *ca.* 516 eV. This peak is attributed to the presence of V^{4+}, which is commonly observed in the hydrated form of V_2O_5[72] as well as in reduced films.[73] But, it is not present in a crystalline V_2O_5 film that has been subjected to thermal evaporation or annealed at high temperatures, as these procedures eliminate all water.[72] This shoulder at 516 eV has also been observed by Ziberberg *et al.*, in the XPS analyses of a V_2O_5 thin film (10 nm) obtained from vanadium(v)-oxytriisopropoxide (ViPr). However, they attributed the presence of the V^{4+} peak to air exposure and not to any possible organic residues from the ViPr (despite having observed residual carbon by XPS).

The calculated composition analyses of the films show that V^{4+} accounts for a very small amount (less than 10% of total V), indicating that both thin films are partially reduced if compared to the stoichiometric V_2O_5. Taking into account the atomic ratio of V and O (expected V : O ratio of 1 : 2.46 for V_2O_5), we can be aware of the content of oxygen vacancies in the films. A deviation from the stoichiometric V : O ratio, of 1 : 2.46, was observed for both films, an indication of the presence of oxygen vacancies that arise from the reduction of V_2O_5, as expected.[72] Moreover, the peak at 533.2 eV of the O 1s is slightly higher in intensity for the film made from the freshly prepared solution, and almost disappears in the thin film made from the aged

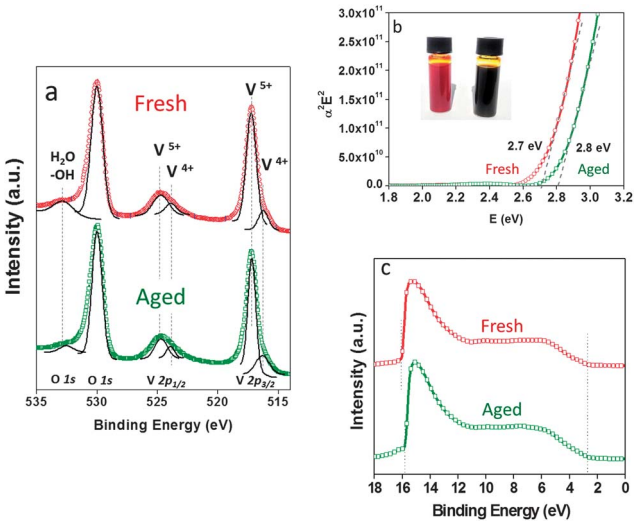

Fig. 4 XPS (a), band gap (b) and UPS (c) spectra of the $V_2O_5 \cdot 0.5H_2O$ thin film obtained from freshly prepared (red) or 24 h-old (green) V_2O_5–IPA solution.

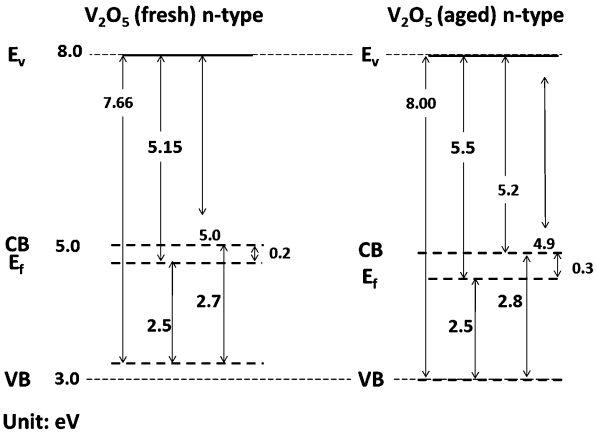

Fig. 5 Band diagrams for V_2O_5 thin films obtained from freshly prepared (a) or 24 h-old and (b) V_2O_5–IPA solutions. E_v: vacuum level; CB: conduction band; E_f: Fermi level; and VB: valence band.

V_2O_5–IAP solution (as can be seen in Fig. 4a and S3†). This is in good agreement with the replacement of the water molecules intercalated in V_2O_5 by the IAP molecules in solution. Once prepared as a thin film, the IAP evaporates from the V_2O_5 layer leaving behind a thin film without (or at least less amount) of water molecules.

We can infer from these results that both thin films are partially reduced: the film prepared with fresh solution, by water, and the film prepared with the 24 h-old solution, by IPA.

The optical band gap (BG), calculated from Tauc's formula, plot of α^2E^2 against photo energy,[75] is shown in Fig. 4b. It reveals a slight difference in BGs between the thin films fabricated from either fresh (red) or 24 h-old (green) V_2O_5–IPA solution, with values of 2.7 eV and 2.8 eV, respectively. The full He I scan of the ultraviolet photoelectron spectroscopy (UPS) analyses of the films is shown in Fig. 4c. The work function (WF) values obtained were 5.15 eV (fresh) and 5.5 eV (24 h-old), respectively, as reflected in the photoemission offset around 16 eV. These values are in good agreement with WF values of thin films of V_2O_5 fabricated in air.[15] Finally, the values for the ionisation potential (IP), defined as the energy difference between the valence band (VB) edge and the vacuum level (E_v), are 7.66 eV (fresh) and 8.0 eV (24 h-old).

These results permitted the construction of the band energy diagram for both thin films as shown in Fig. 5. To calculate the voltage of the OSC, we used the LUMO level of ZnO at 4.4 eV[57] and the HOMO level obtained experimentally for V_2O_5 at 5.0 to 5.16 eV. The latter yields a V_{oc} value of 0.56 V to 0.6 V, which is in good agreement with the experimental V_{oc} values obtained for the OSCs shown in Fig. 3 (and very similar to the V_{oc} values between 0.56 and 0.58 V observed in Fig. 1). However, we were unable to arrive at a clear conclusion regarding the V_{oc} value of the solar cell that contained the V_2O_5 thin film made from the 24 h-old (green) V_2O_5–IPA solution (experimentally 0.38 V) since there is a wide range of possible reduction stages for V_2O_5 that can be detected in IPA over time. Thus, based on the experimental and calculated values of V_{oc}, we reasoned that the fabrication steps followed to obtain the V_2O_5 thin film affect the final photovoltaic response of the OSC. Moreover, the final V_{oc} of the device is probably chiefly dictated by the semiconductor oxide layers and by the HOMO/LUMO levels of the donor and acceptor materials of the active P3HT:PCBM layer.

3.3 OSCs with normal and inverted configuration with an Ag back metal electrode

One of the limitations for the fabrication of normal-configuration OSCs by low-temperature solution processing techniques is the requirement of low work function back metal electrodes, such as Al.[10,58] While Ag electrodes can easily be printed from solution, there is currently no viable route for printing a stable Al electrode.[10] This is a drawback that also limits the manufacture, by printing techniques, of tandem or multi-junction OSCs in the normal-configuration. Thus, in this section, we want to demonstrate that the fabrication of OSCs applying an Ag metal electrode is possible for both configurations when the V_2O_5 HTL is applied.

Fig. 6 shows the solar cells' energy band diagrams (a and b), the solar cell architectures in both configurations (c and d), and the corresponding *IV* curves and IPCE analyses for both types of devices (e and f). The photovoltaic parameters obtained are detailed in Table 3. The band energy diagrams in Fig. 6a and b are represented in relation to the relative energy levels of the acceptor (PCBM) and the donor (P3HT). The experimental values observed for the V_2O_5 thin film (5.1 eV) are very close to the energy level of the P3HT, and in good agreement with the work function of the Ag and the FTO electrodes responsible for the hole and electron collection respectively. Comparison of the photovoltaic response indicates a very similar behaviour, with V_{oc} ranging between 0.54 V and 0.56 V and the FF between 47 and 48%. The main difference is observed on the J_{sc}, which is lower for the OSC in the normal configuration in comparison with the inverted configuration. The difference in J_{sc} also limits the PCEs, which is observed between 2.6% and 3% for the inverted configuration, and at around 2% for the normal configuration (see Table 3). This difference in PCE is further validated by the

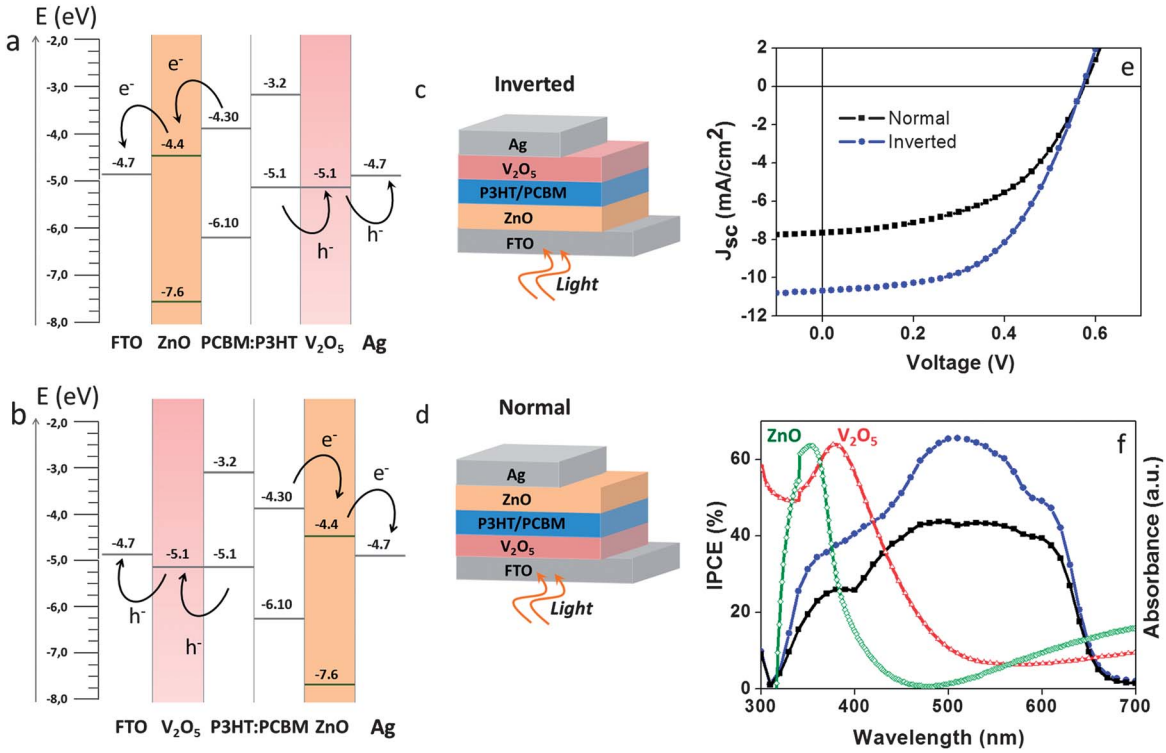

Fig. 6 Schematic representation of the band energy diagram for the inverted (a) and normal (b) configuration of organic solar cells containing ZnO as the electron transport layer and water-based, solution-processed V_2O_5 as the hole transport layer. The architecture of the inverted (e) and the normal (d) configuration OSCs. *IV* curves (c) and IPCE spectra (f) of the OSCs in each configuration. In both cases, an Ag back metal electrode was used. Measurements were taken at 100 mW cm^{-2} AM1.5G.

Table 3 Photovoltaic parameters of OSCs in the normal or the inverted configuration, with an Ag back metal electrode and water-based, solution-processed V_2O_5 as the hole transport layer. Measurements were taken at 100 mW cm^{-2} AM1.5G[a]

Device structure	V_{oc} (V)	J_{sc} (mA cm^{-2})	FF (%)	PCE (%)
Inverted Glass/FTO/ZnO/ P3HT:PCBM/ V_2O_5/Ag	0.540 ± 0.01	9.54 ± 1.1	47.20 ± 1.9	2.58 ± 0.2
Normal Glass/FTO/V_2O_5/ P3HT:PCBM/ ZnO/Ag	0.565 ± 0.01	7.65 ± 0.3	48.35 ± 2.3	2.10 ± 0.2
Reference cell Glass/FTO/TiO_2/ P3HT:PCBM/ V_2O_5/Ag	0.563 ± 0.01	10.69 ± 0.3	50.49 ± 1.9	3.09 ± 0.1

[a] Average value from six samples.

corresponding IPCE responses: with 70% and 40% for inverted and the normal configuration, respectively. The dissimilarity in the performance between the two types of OSCs can be attributed to the greater light reflection and the UV-filter effect imposed by the V_2O_5 layer on the device. In the case where the device is illuminated from the FTO/V_2O_5 side (see Fig. 6d and e), the V_2O_5 layer could be acting as a UV-filter, limiting the amount of light reaching the cell. Adsorption spectra of the ZnO and the V_2O_5 layers are shown in Fig. 6f. V_2O_5 adsorbs at wavelengths up to 450 nm while in the inverted configuration (Fig. 6c), light enters the device from the FTO/ZnO side, where the ZnO layer blocks only the UV wavelength region below 380 nm. An interesting aspect observed is the value of V_{oc} that is almost the same for both types of devices. This is an indication that the LUMO level of ZnO at 4.4 eV and the HOMO level of V_2O_5 at 5.16 eV can be used to calculate the V_{oc} of the normal configuration OSC.[57] In the same way it was described before for the inverted OSC in Section 3.2. OSCs applying V_2O_5 as the HTL[5,10,13,14,16–20,81–83] have been usually reported with an Ag metal electrode in the inverted configuration,[5,10,15,57] and an Al or Ca electrode in the normal configuration.[14,19,21,58] In our work, the photovoltaic response of both types of OSCs seems to be independent of the Ag back metal electrode employed. This makes the OSCs amenable to fabrication by printing methods as the Ag metal electrode can simply be printed from solution.[5,10,44,79] This also could be a step forward to the fabrication of more compatible recombination layers for TmOSCs.[10]

The selection of the adequate back metal electrode in OSCs has been the subject of extensive research work. The OSCs that have been studied to date contain only one oxide semiconductor used as the ETL (usually TiO_2, TiO_x or ZnO), and PEDOT:PSS as the HTL.[44,84] Since the use of TMOs as both ETL and HTL is relatively new, we have not found any other work in which a high work-function metal electrode (*e.g.* Ag) is used for

the normal configuration OSC. Greiner *et al.* recently described the effect of metal electrodes on the work function and band structure of MoO_3 at metal/metal oxide interfaces. The reduction of the oxide (from Mo^{6+} to Mo^{3+}) in contact with the metal electrode results in a lower work function of the oxide, and the maximum value depends on the thickness of the oxide layer.[85] Hadipour *et al.* have employed an Ag metal electrode in different OSCs in the normal configuration, including the ones in which MoO_3 is the HTL. However, a thin layer of Ca between the active layer of P3HT:PCBM and the Ag metal electrode was employed for the normal configuration OSCs.[86] Lidzey *et al.* have reported a study on different back metal electrodes in normal configuration OSCs in which MoO_3 is also the HTL.[87] The authors fabricated OSCs of the type ITO/MoO_3/PCDTBT:$PC_{70}BM$/metal electrode (note that no ETL was applied between the active layer and the metal electrode), using diverse, thermally evaporated metals (Ag, Al, Ca, Ca/Ag and Ca/Al). The final photovoltaic performance of the solar cells was very similar in all cases, showing only slight differences among the devices. The authors chose the Ca/Al back electrode as the best one, owing to its slightly better photovoltaic response. Although their work involved only one TMO as the HTL (MoO_3) and did not entail the use of any ETL, it is the closest research work related to the one presented here by us (in terms of set-up and results). It also supports the idea that the photovoltaic performance of normal configuration OSCs containing metal oxides is probably independent of the back metal electrode used. Despite the advances made by Lidzey *et al.*, our group and others, substantial studies are needed to clarify the role of the back electrode in these TMO-based OSCs.

3.4 Outdoor stability analyses: normal *vs.* inverted OSCs, effects of UV filter

The lifetime stability of the OSCs was analyzed under outdoor conditions for 1000 h. Fig. 7 shows the normalized PCE response observed with time for the inverted and normal configuration OSCs applying V_2O_5 as the HTL. Initial results revealed that the light irradiation dose affects drastically the OSCs' response as can be observed in Fig. 7. A peak on PCE can be observed almost every time the light irradiation drops below 1 sun (100 W m^{-2}), especially for irradiance between 0.6 and 0.8 suns (see also ESI, Fig. S4 and S5†). Moreover, the lifetime analyses revealed better stability and longer lifetimes for OSCs with normal-configuration, staying at T_{80} even after 1000 h of analysis. The inverted-configuration OSCs revealed strong degradation reaching T_{80} after only 320 h of analysis. This response was unexpected since the OSCs with inverted-configuration are well-known to display higher stability (even under ambient conditions) than the normal configuration OSCs.[47–50,88] In our solar cells, we consider that the greater stability of the normal configuration OSC is partly due to the UV-filter effect that the V_2O_5 layer can impose on the device when illuminated from the FTO/V_2O_5 side, as already described.

In order to demonstrate that the OSCs would be more stable in the absence of UV light, we applied a UV filter to the inverted-configuration OSC. Two samples, one with the UV filter and the other without, were analysed outdoors under the same conditions. The filter (an adhesive UV filter film that cuts UV light below 400 nm) was applied on top of the test cell. Fig. 7b shows the observed response for the first 1000 h of analysis. The control sample performed just like the inverted OSC analysed in Fig. 7a, reaching T_{60} at ~500 h and T_{40} at ~1000 h. However, the sample with the UV filter remained at T_{80} for many hours and was still stable after ~1000 h of testing. Thus we can demonstrate that elimination of UV light can improve the lifetime of the inverted-configuration OSC by several orders of magnitude.

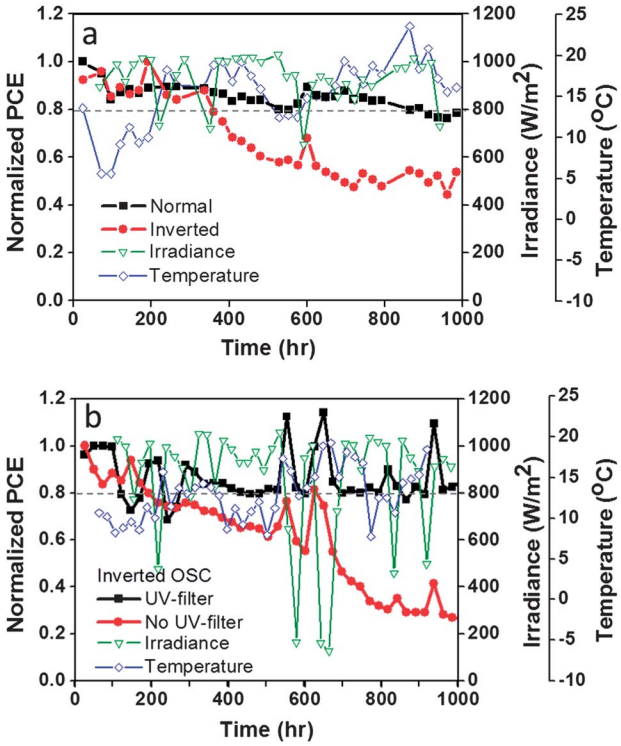

Fig. 7 Outdoor stability analysis of sealed OSCs containing water-based, solution-processed V_2O_5 as the hole transport layer. Comparison of normalised PCE response: (a) normal configuration *vs.* inverted configuration (both without the UV filter); and (b) with the UV filter *vs.* without the UV filter (both in inverted configuration). The cells were analysed outdoors in Barcelona, Spain (41.30° N, 2.09° W). The PCE values were calculated using the maximum irradiance level per day. Average temperatures: 10 to 15 °C (day) and 5 to 7 °C (night). Average RH: 70%. Normal configuration: glass/FTO/V_2O_5/P3HT:PCBM/ZnO/Ag. Inverted configuration: glass/FTO/ZnO/P3HT:PCBM/V_2O_5/Ag.

In this work, we have demonstrated the high stability of OSCs containing $V_2O_5 \cdot 0.5H_2O$ as the HTL despite the presence of water molecules in the layer. The degradation of the OSC lacking the UV filter indicates that V_2O_5 is photoactive under UV light, and that the active P3HT:PCBM layer or the Ag electrode can interact with the V_2O_5 HTL. Nevertheless, a UV filter is beneficial and improves the OSC's stability.

4 Conclusions

In summary, we have demonstrated the first example of stable organic solar cells (OSCs) containing a layered V_2O_5 hydrate as the hole transport layer (HTL). V_2O_5 is processed from a water-based solution in air, resulting in a final thin film of formula

$V_2O_5 \cdot 0.5H_2O$. The water molecules remain in the V_2O_5 layered structure at temperatures below 250 °C, which makes the thin film highly stable under real working conditions. The HTL was employed in OSCs in either the normal or the inverted configuration, in which Ag was used for the back metal electrode. These types of OSCs can be fabricated totally by solution-processing printing in air, as they do not require the Al electrode found in normal-configuration OSCs. XPS, UPS and optical characterisation of the V_2O_5 thin films revealed differences based on the age of the V_2O_5–isopropanol (IPA) solution used for film deposition. In films made with a 24 h-old solution, reduction of the oxide (from V^{5+} to V^{4+}) by IPA meant that subsequent re-oxidation (by photo-annealing) was required to achieve optimal photovoltaic performance. In contrast, the films made with fresh V_2O_5–isopropanol solution directly exhibited peak performance and therefore did not require any photo-annealing. The normal-configuration OSCs do not require any photo-annealing because the V_2O_5 thin film is formed from an aqueous solution. Outdoor stability analyses of sealed OSCs containing V_2O_5 as the HTL, in either the inverted or the normal configuration, revealed that the normal-configuration was highly stable. It remained at T_{80} even after 1000 h, probably due to the fact that it is illuminated from the FTO/V_2O_5 side and to the UV-filtering effect of the V_2O_5 layer. In contrast, the inverted-configuration OSC, which is illuminated from the FTO/ZnO side, was far less stable. Our hypothesis on the effects of the V_2O_5 layer was corroborated by a subsequent test in which an inverted-configuration OSC, equipped with an external UV-filter, achieved comparable levels of stability to that of the normal-configuration OSC.

Acknowledgements

We thank Aurelie Vanwaelscappel for the AFM image. We thank Guillaume Sauthier for his advice on the XPS and UPS analyses, and Prof. Frederik C. Krebs from the Technical University of Denmark (DTU) for providing the sample of the adhesive UV-filter employed for the stability/lifetime testing. We thank CONACYT (Mexico) for the PhD scholarship for G. T. E., the Erasmus fellowship programme for financial support for J. P., the Spanish Ministry of Economy and Competitively (MINECO) for the Consolider grant NANOSELECT CSD2007-00041, and the Xarxa de Referència en Materials Avançats per a l'Energia, XaRMAE (Reference Centre for Advanced Materials for Energy) of the Catalan government.

Notes and references

1 R. A. J. Janssen and J. Nelson, *Adv. Mater.*, 2013, **25**, 1847–1858.
2 H. Hoppe and N. S. Sariciftci, *J. Mater. Res.*, 2004, **19**, 1924–1945.
3 F. C. Krebs, S. A. Gevorgyan and J. Alstrup, *J. Mater. Chem.*, 2009, **19**, 5442–5451.
4 M. R. Lilliedal, A. J. Medford, M. V. Madsen, K. Norrman and F. C. Krebs, *Sol. Energy Mater. Sol. Cells*, 2010, **94**, 2018–2031.
5 T. T. Larsen-Olsen, T. R. Andersen, B. Andreasen, A. P. L. Böttiger, E. Bundgaard, K. Norrman, J. W. Andreasen, M. Jørgensen and F. C. Krebs, *Sol. Energy Mater. Sol. Cells*, 2012, **97**, 43–49.
6 E. Lee, J. Kim and C. Kim, *Sol. Energy Mater. Sol. Cells*, 2012, **105**, 1–5.
7 Z. Tan, L. Li, C. Cui, Y. Ding, Q. Xu, S. Li, D. Qian and Y. Li, *J. Phys. Chem. C*, 2012, **116**, 18626–18632.
8 S. R. Dupont, E. Voroshazi, P. Heremans and R. H. Dauskardt, *Org. Electron.*, 2013, **14**, 1262–1270.
9 O. Hagemann, M. Bjerring, N. C. Nielsen and F. C. Krebs, *Sol. Energy Mater. Sol. Cells*, 2008, **92**, 1327–1335.
10 T. T. Larsen-Olsen, E. Bundgaard, K. O. Sylvester-Hvid and F. C. Krebs, *Org. Electron.*, 2011, **12**, 364–371.
11 R. Søndergaard, M. Helgesen, M. Jørgensen and F. C. Krebs, *Adv. Energy Mater.*, 2011, **1**, 68–71.
12 N. Espinosa, H. F. Dam, D. M. Tanenbaum, J. W. Andreasen, M. Jørgensen and F. C. Krebs, *Materials*, 2011, **4**, 169–182.
13 W. T. Chiang, S. H. Su, Y. F. Lin and M. Yokoyama, *Jpn. J. Appl. Phys.*, 2010, **49**, O4DK14.
14 K. Zilberberg, S. Trost, H. Schmidt and T. Riedl, *Adv. Energy Mater.*, 2011, **1**, 377–381.
15 K. Zilberberg, S. Trost, J. Meyer, A. Kahn, A. Behrendt, D. Lützenkirchen-Hecht, R. Frahm and T. Riedl, *Adv. Funct. Mater.*, 2011, **21**, 4776–4783.
16 S. R. Dupont, M. Oliver, F. C. Krebs and R. H. Dauskardt, *Sol. Energy Mater. Sol. Cells*, 2012, **97**, 171–175.
17 C. Gong, H. B. Yang, Q. L. Song and C. M. Li, *Org. Electron.*, 2012, **13**, 7–12.
18 S. H. Su, W. K. Lin, W. T. Chiang, Y. F. Lin and M. Yokoyama, *Jpn. J. Appl. Phys.*, 2012, **51**, 02BK03.
19 H. Q. Wang, N. Li, N. S. Guldal and C. J. Brabec, *Org. Electron.*, 2012, **13**, 3014–3021.
20 M. Hajzeri, A. S. Vuk, L. S. Perse, M. Colovic, B. Herbig, U. Posset, M. Krzmanc and B. Orel, *Sol. Energy Mater. Sol. Cells*, 2012, **99**, 67–72.
21 F. Xie, W. C. H. Choy, C. Wang, X. Li, S. Zhang and J. Hou, *Adv. Mater.*, 2013, **25**, 2051–2055.
22 J. C. Bernede, S. Houari, D. Nguyen, P. Y. Jouan, A. Khelil, A. Mokrani, L. Cattin and P. Predeep, *Phys. Status Solidi A*, 2012, **209**, 1291–1297.
23 R. Betancur, M. Maymóc, X. Elias, L. T. Vuong and J. Martorell, *Sol. Energy Mater. Sol. Cells*, 2011, **95**, 735–739.
24 Q. Chen, B. J. Worfolk, T. C. Hauger, U. Al-Atar, K. D. Harris and J. M. Buriak, *ACS Appl. Mater. Interfaces*, 2011, **3**, 3962–3970.
25 M. D. Irwin, B. Buchholz, A. W. Hains, R. P. H. Chang and T. J. Marks, *Proc. Natl. Acad. Sci. U. S. A.*, 2008, **105**, 2783–2787.
26 M. D. Irwin, J. D. Servaites, D. B. Buchholz, B. J. Leever, J. Liu, J. D. Emery, M. Zhang, J. H. Song, M. F. Durstock, A. J. Freeman, M. J. Bedzyk, M. C. Hersam, R. P. H. Chang, M. A. Ratner and T. J. Marks, *Chem. Mater.*, 2011, **23**, 2218–2226.
27 C. H. Poh, C. K. Poh, G. Bryant, W. Belcher and P. Dastoor, *Proc. SPIE*, 2011, **8204OW**.
28 K. X. Steirer, J. P. Chesin, N. E. Widjonarko, J. J. Berry, A. Miedaner, D. S. Ginley and D. C. Olson, *Org. Electron.*, 2010, **11**, 1414–1418.

29 K. X. Steirer, P. F. Ndione, N. E. Widjonarko, M. T. Lloyd, J. Meyer, E. L. Ratcliff, A. Kahn, N. R. Armstrong, C. J. Curtis, D. S. Ginley, J. J. Berry and D. C. Olson, *Adv. Energy Mater.*, 2011, **1**, 813–820.
30 N. Sun, G. Fang, P. Qin, Q. Zheng, M. Wang, X. Fan, F. Cheng, J. Wan and X. Zhao, *Sol. Energy Mater. Sol. Cells*, 2010, **94**, 2328–2331.
31 D. W. Zhao, P. Liu, X. W. Sun, S. T. Tan, L. Ke and A. K. K. Kyaw, *Appl. Phys. Lett.*, 2009, **95**, 153304.
32 A. K. K. Kyaw, X. W. Sun, C. Y. Jiang, G. Q. Lo, D. W. Zhao and D. L. Kwong, *Appl. Phys. Lett.*, 2008, **93**.
33 Y. Kinoshita, R. Takenaka and H. Murata, *Appl. Phys. Lett.*, 2008, **92**, 243309.
34 C. Girotto, E. Voroshazi, D. Cheyns, P. Heremans and B. P. Rand, *ACS Appl. Mater. Interfaces*, 2011, **3**, 3244–3247.
35 H. Schmidt, H. Flügge, T. Winkler, T. Bülow, T. Riedl and W. Kowalsky, *Appl. Phys. Lett.*, 2009, **94**, 243302.
36 A. G. F. Janssen, T. Riedl, S. Hamwi, H. H. Johannes and W. Kowalsky, *Appl. Phys. Lett.*, 2007, **91**, 073519.
37 C. Tao, S. Ruan, G. Xie, X. Kong, L. Shen, F. Meng, C. Liu, X. Zhang, W. Dong and W. Chen, *Appl. Phys. Lett.*, 2009, **94**, 043311.
38 C. Tao, G. Xie, F. Meng, S. Ruan and W. Chen, *J. Phys. Chem. C*, 2011, **115**, 12611–12615.
39 M. G. Varnamkhasti, H. R. Fallah, M. Mostajaboddavati, R. Ghasemi and A. Hassanzadeh, *Sol. Energy Mater. Sol. Cells*, 2012, **98**, 379–384.
40 L. J. Zuo, X. X. Jiang, L. G. Yang, M. S. Xu, Y. X. Nan, Q. X. Yan and H. Z. Chen, *Appl. Phys. Lett.*, 2011, **99**, 183306.
41 M. T. Greiner, M. G. Helander, W.-M. Tang, Z.-B. Wang, J. Qiu and Z.-H. Lu, *Nat. Mater.*, 2012, **11**, 76–81.
42 H. Ma, H. L. Yip, F. Huang and A. K. Y. Jen, *Adv. Funct. Mater.*, 2010, **20**, 1371–1388.
43 W. J. Potscavage Jr, A. Sharma and B. Kippelen, *Acc. Chem. Res.*, 2009, **42**, 1758–1767.
44 R. Steim, F. R. Kogler and C. J. Brabec, *J. Mater. Chem.*, 2010, **20**, 2499–2512.
45 Z. B. Wang, M. G. Helander, M. T. Greiner, J. Qiu and Z. H. Lu, *Phys. Rev. B: Condens. Matter Mater. Phys.*, 2009, **80**, 235325.
46 K. Norrman, M. V. Madsen, S. A. Gevorgyan and F. C. Krebs, *J. Am. Chem. Soc.*, 2010, **132**, 16883–16892.
47 B. Andreasen, D. M. Tanenbaum, M. Hermenau, E. Voroshazi, M. T. Lloyd, Y. Galagan, B. Zimmernann, S. Kudret, W. Maes, L. Lutsen, D. Vanderzande, U. Wurfel, R. Andriessen, R. Rosch, H. Hoppe, G. Teran-Escobar, M. Lira-Cantu, A. Rivaton, G. Y. Uzunoglu, D. S. Germack, M. Hosel, H. F. Dam, M. Jorgensen, S. A. Gevorgyan, M. V. Madsen, E. Bundgaard, F. C. Krebs and K. Norrman, *Phys. Chem. Chem. Phys.*, 2012, **14**, 11780–11799.
48 R. Rosch, D. M. Tanenbaum, M. Jorgensen, M. Seeland, M. Barenklau, M. Hermenau, E. Voroshazi, M. T. Lloyd, Y. Galagan, B. Zimmermann, U. Wurfel, M. Hosel, H. F. Dam, S. A. Gevorgyan, S. Kudret, W. Maes, L. Lutsen, D. Vanderzande, R. Andriessen, G. Teran-Escobar, M. Lira-Cantu, A. Rivaton, G. Y. Uzunoglu, D. Germack, B. Andreasen, M. V. Madsen, K. Norrman, H. Hoppe and F. C. Krebs, *Energy Environ. Sci.*, 2012, **5**, 6521–6540.
49 D. M. Tanenbaum, M. Hermenau, E. Voroshazi, M. T. Lloyd, Y. Galagan, B. Zimmermann, M. Hosel, H. F. Dam, M. Jorgensen, S. A. Gevorgyan, S. Kudret, W. Maes, L. Lutsen, D. Vanderzande, U. Wurfel, R. Andriessen, R. Rosch, H. Hoppe, G. Teran-Escobar, M. Lira-Cantu, A. Rivaton, G. Y. Uzunoglu, D. Germack, B. Andreasen, M. V. Madsen, K. Norrman and F. C. Krebs, *RSC Adv.*, 2012, **2**, 882–893.
50 G. Teran-Escobar, D. M. Tanenbaum, E. Voroshazi, M. Hermenau, K. Norrman, M. T. Lloyd, Y. Galagan, B. Zimmermann, M. Hosel, H. F. Dam, M. Jorgensen, S. Gevorgyan, S. Kudret, W. Maes, L. Lutsen, D. Vanderzande, U. Wurfel, R. Andriessen, R. Rosch, H. Hoppe, A. Rivaton, G. Y. Uzunoglu, D. Germack, B. Andreasen, M. V. Madsen, E. Bundgaard, F. C. Krebs and M. Lira-Cantu, *Phys. Chem. Chem. Phys.*, 2012, **14**, 11824–11845.
51 F. J. Zhang, D. W. Zhao, Z. L. Zhuo, H. Wang, Z. Xu and Y. S. Wang, *Sol. Energy Mater. Sol. Cells*, 2010, **94**, 2416–2421.
52 D. Y. Kim, G. Sarasqueta and F. So, *Sol. Energy Mater. Sol. Cells*, 2009, **93**, 1452–1456.
53 J. Li, Q. Y. Bao, H. X. Wei, Z. Q. Xu, J. P. Yang, Y. Q. Li, S. T. Lee and J. X. Tang, *J. Mater. Chem.*, 2012, **22**, 6285–6290.
54 S. Kouijzer, S. Esiner, C. H. Frijters, M. Turbiez, M. M. Wienk and R. A. J. Janssen, *Adv. Energy Mater.*, 2012, **2**, 945–949.
55 V. S. Gevaerts, A. Furlan, M. M. Wienk, M. Turbiez and R. A. J. Janssen, *Adv. Mater.*, 2012, **24**, 2130–2134.
56 Y. Yuan, J. Huang and G. Li, *Green*, 2011, **1**, 65–80.
57 C. P. Chen, Y. D. Chen and S. C. Chuang, *Adv. Mater.*, 2011, **23**, 3859–3863.
58 I. Hancox, L. A. Rochford, D. Clare, M. Walker, J. J. Mudd, P. Sullivan, S. Schumann, C. F. McConville and T. S. Jones, *J. Phys. Chem. C*, 2013, **117**, 49–57.
59 D. Gupta, M. M. Wienk and R. A. J. Janssen, *Adv. Energy Mater.*, 2013, **3**, 782–787.
60 M. Lira-Cantu and F. C. Krebs, *Sol. Energy Mater. Sol. Cells*, 2006, **90**, 2076–2086.
61 I. Gonzalez-Valls and M. Lira-Cantu, *Energy Environ. Sci.*, 2010, **3**, 789–795.
62 J. Livage, *Chem. Mater.*, 1991, **3**, 578–593.
63 M. O. Reese, S. A. Gevorgyan, M. Jørgensen, E. Bundgaard, S. R. Kurtz, D. S. Ginley, D. C. Olson, M. T. Lloyd, P. Morvillo, E. A. Katz, A. Elschner, O. Haillant, T. R. Currier, V. Shrotriya, M. Hermenau, M. Riede, K. R. Kirov, G. Trimmel, T. Rath, O. Inganäs, F. Zhang, M. Andersson, K. Tvingstedt, M. Lira-Cantu, D. Laird, C. McGuiness, S. Gowrisanker, M. Pannone, M. Xiao, J. Hauch, R. Steim, D. M. DeLongchamp, R. Rösch, H. Hoppe, N. Espinosa, A. Urbina, G. Yaman-Uzunoglu, J.-B. Bonekamp, A. J. J. M. van Breemen, C. Girotto, E. Voroshazi and F. C. Krebs, *Sol. Energy Mater. Sol. Cells*, 2011, **95**, 1253–1267.
64 J. Livage, *Coord. Chem. Rev.*, 1998, **178–180**, 999–1018.
65 M. Nabavi, C. Sanchez and J. Livage, *Eur. J. Solid State Inorg. Chem.*, 1991, **28**, 1173–1192.
66 J. Livage, *Mater. Res. Bull.*, 1991, **26**, 1173–1180.
67 J. Livage, *Coord. Chem. Rev.*, 1999, **190–192**, 391–403.
68 J. Livage, F. Beteille, C. Roux, M. Chatry and P. Davidson, *Acta Mater.*, 1998, **46**, 743–750.

69 S. Kittaka, H. Yamamoto, S. Higuma and T. Sasaki, *J. Chem. Soc., Faraday Trans.*, 1992, **88**, 715–718.
70 M. Jørgensen, K. Norrman, S. A. Gevorgyan, T. Tromholt, B. Andreasen and F. C. Krebs, *Adv. Mater.*, 2012, **24**, 580–612.
71 A. Manor, E. A. Katz, T. Tromholt and F. C. Krebs, *Sol. Energy Mater. Sol. Cells*, 2012, **98**, 491–493.
72 V. Bondarenka, S. Kaciulis, Z. Martunas, A. Reza, G. J. Babonas and A. Pasiskevicius, *Lith. J. Phys.*, 2008, **48**, 341–348.
73 J. Świątowska-Mrowiecka, F. Martin, V. Maurice, S. Zanna, L. Klein, J. Castle and P. Marcus, *Electrochim. Acta*, 2008, **53**, 4257–4266.
74 D. Liu, Y. Liu, B. B. Garcia, Q. Zhang, A. Pan, Y. H. Jeong and G. Cao, *J. Mater. Chem.*, 2009, **19**, 8789–8795.
75 M. Benmoussa, A. Outzourhit, R. Jourdani, A. Bennouna and E. L. Ameziane, *Act. Passive Electron. Compon.*, 2003, **26**, 245–256.
76 J. Meyer, K. Zilberberg, T. Riedl and A. Kahn, *J. Appl. Phys.*, 2011, **110**, 033710.
77 Z. Y. Li and Q. H. Wu, *J. Mater. Sci.: Mater. Electron.*, 2008, **19**, S366–S370.
78 A. L. Pergament, E. L. Kazakova and G. B. Stefanovich, *J. Phys. D: Appl. Phys.*, 2002, **35**, 2187–2197.
79 H. L. Yip and A. K. Y. Jen, *Energy Environ. Sci.*, 2012, **5**, 5994–6011.
80 I. Gonzalez-Valls, D. Angmo, S. A. Gevorgyan, J. Sebastián Reparaz, F. C. Krebs and M. Lira-Cantu, *J. Polym. Sci., Part B: Polym. Phys.*, 2013, **51**, 272–280.
81 P. Lutsyk and Y. Vertsimakha, *Mol. Cryst. Liq. Cryst.*, 2005, **426**, 265–276.
82 G. Li, C. W. Chu, V. Shrotriya, J. Huang and Y. Yang, *Appl. Phys. Lett.*, 2006, **88**, 253503.
83 A. Ojala, H. Burckstummer, J. Hwang, K. Graf, B. von Vacano, K. Meerholz, P. Erk and F. Wurthner, *J. Mater. Chem.*, 2012, **22**, 4473–4482.
84 E. D. Gomez and Y. L. Loo, *J. Mater. Chem.*, 2010, **20**, 6604–6611.
85 M. T. Greiner, L. Chai, M. G. Helander, W. M. Tang and Z. H. Lu, *Adv. Funct. Mater.*, 2013, **23**, 215–226.
86 A. Hadipour, D. Cheyns, P. Heremans and B. P. Rand, *Adv. Energy Mater.*, 2011, **1**, 930–935.
87 D. C. Watters, J. Kingsley, H. Yi, T. Wang, A. Iraqi and D. Lidzey, *Org. Electron.*, 2012, **13**, 1401–1408.
88 E. Voroshazi, B. Verreet, A. Buri, R. Müller, D. Di Nuzzo and P. Heremans, *Org. Electron.*, 2011, **12**, 736–744.